JOURNAL OF THE AMERICAN CHEMICAL SOCIETY

pubs.acs.org/JACS Article

Dynamic Interconversion of Ga(III) and GaH_x in Ga-MFI Zeolites for Efficient CO_2−Cyclohexane Coupling Conversion to Aromatics

Haohao Feng, Zhong-Pan Hu, Enze Chen, Yimo Wu, Min Li, Jingfeng Han,* Yingxu Wei, and Zhongmin Liu*

Cite This: *J. Am. Chem. Soc.* 2025, 147, 32915−32923

Read Online

ACCESS | Metrics & More | Article Recommendations | Supporting Information

Downloaded via DALIAN INST OF CHEMICAL PHYSICS on September 16, 2025 at 01:07:12 (UTC).
See https://pubs.acs.org/sharingguidelines for options on how to legitimately share published articles.

ABSTRACT: The catalytic coupling conversion of naphtha and CO_2 to aromatics over metal-zeolites offers a fascinating route for aromatics production, yet, the exploitation of efficient metal-zeolite catalysts and CO_2 coupled naphtha to make CO_2 transformed into high-value-added chemicals remain great challenges. Herein, we synthesized a framework-anchored Ga-MFI catalyst synthesized *via* ligand-assisted hydrothermal crystallization, achieving 80.76% aromatic selectivity at 99.57% cyclohexane conversion (550 °C, 0.1 MPa, WHSV = 1 h^{-1}) with over 110 h stability for CO_2 and cyclohexane (as a model naphthenic compound) coupling reaction. Multimodal *in situ* characterization (XAFS, synchrotron XRD, and FTIR) reveals that isolated Ga(III) species undergo reversible coordination switching to GaH_x under reaction conditions, dynamically mediating CO_2 activation through Ga species transfer. Tetrahedrally coordinated Ga−O sites synergize with proximal Brønsted acid sites. Isotopic tracing ($^{13}CO_2$) demonstrates 56.4% of aromatic carbon originates. The catalyst's self-recovery capability ensures structural integrity and suppresses deactivation. This work establishes a dynamic single-site catalysis framework for a CO_2 coupled alkane, advancing the design of zeolite-confined metal catalysts through precise microenvironment engineering.

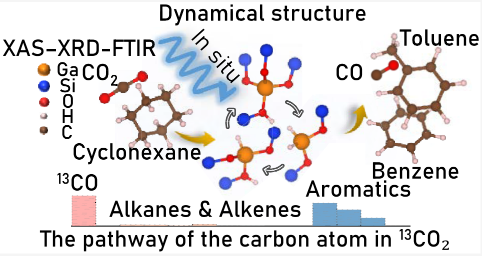

1. INTRODUCTION

Naphtha is a basic feedstock for the petrochemical industry,[1−3] supplying hydrocarbons that undergo catalytic transformations into benzene, toluene, and xylene.[4,5] These aromatic compounds are essential for polymer synthesis and specialty chemicals.[6,7] Conventional metal-catalyzed aromatization processes, however, remain energy-intensive, often requiring temperatures exceeding 600 °C while achieving suboptimal atom economy.[8,9] These systemic inefficiencies amplify the environmental burden of chemical manufacturing, particularly when juxtaposed with escalating global mandates for CO_2 emission mitigation.[10,11]

The urgency to repurpose CO_2, a greenhouse gas with relentlessly rising atmospheric levels, has catalyzed innovations in its synergistic coupling conversion with hydrocarbons.[12,13] CO_2-coupled alkane aromatization, abundant in petroleum fractions, offers platforms for CO_2 valorization.[14,15] Specifically, using CO_2 not only enables the conversion of waste CO_2 into valuable chemicals but also enhances the overall energy efficiency of the process by reducing the need for external hydrogen or high temperatures. Early breakthroughs demonstrated that molecular sieves like H-ZSM-5 could leverage CO_2 as a mild oxidant to enhance aromatic yields in *n*-butane conversion,[16,17] while platinum-based bimetallic systems enabled propane dehydrogenation beyond thermodynamic limits through CO_2-mediated pathways.[18−20] Despite these advances, practical implementation faces intractable compromises: noble metal catalysts impose prohibitive costs, whereas transition metal oxides degrade rapidly under cyclic redox stresses.[21,22]

Gallium-incorporated zeolites have recently garnered attention as redox-adaptive catalysts capable of circumventing these limitations.[23,24] The chameleonic nature of Ga species, which can fluctuate between oxidized and hydridic states under reaction conditions, suggests an intrinsic ability to mediate both C−H activation and CO_2 reduction.[9,25,26] Spectroscopic evidence from reduced Ga/ZSM-5 systems hints at transient Ga−H intermediates as potential active sites, yet their kinetic lability and spatial distribution within zeolite frameworks remain poorly resolved.[27,28] This ambiguity stems partly from the inadequacy of conventional characterization techniques in tracking dynamic metal speciation during operando conditions, a challenge magnified in CO_2−alkane coupling systems demanding precise orchestration of acid−base and redox functionalities.

Our work confronts these dual challenges through the rational design of a framework-anchored Ga-MFI catalyst

Received: June 10, 2025
Revised: August 22, 2025
Accepted: August 25, 2025
Published: August 29, 2025

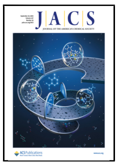

ACS Publications

© 2025 American Chemical Society

https://doi.org/10.1021/jacs.5c09737
J. Am. Chem. Soc. 2025, 147, 32915−32923

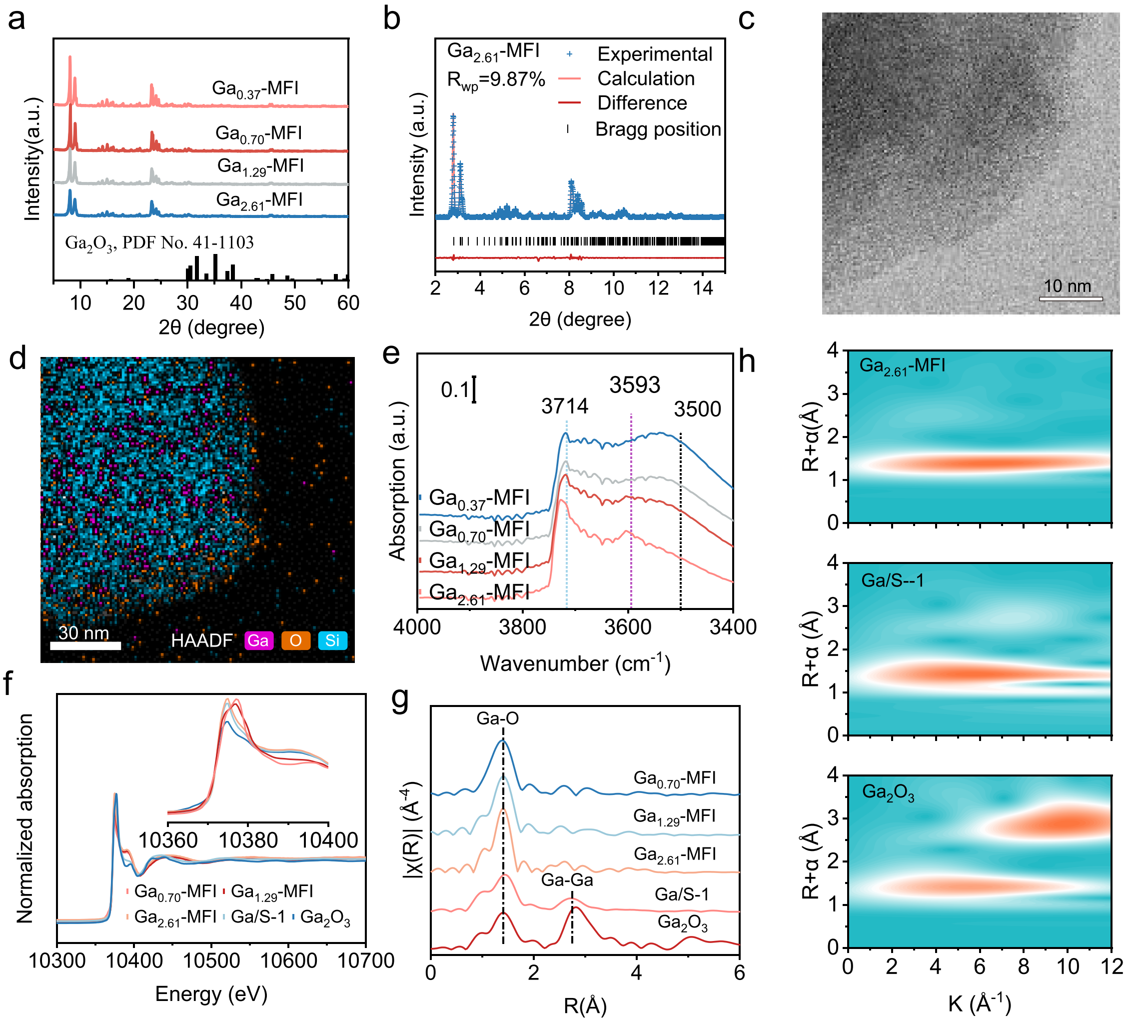

Figure 1. Catalyst structure. (a) XRD patterns of Ga-MFI with different Ga contents, where x represents the Ga content obtained by XRF. (b) Rietveld synchrotron radiation (SR) XRD pattern of $Ga_{2.61}$-MFI (λ = 0.5427 Å). (c) High-angle annular dark-field (HAADF) TEM images of $Ga_{2.61}$-MFI. (d) Elemental mapping image of $Ga_{2.61}$-MFI. (e) Fourier transform infrared spectrum of Ga-MFI with a black background. (f) Normalized XANES spectrum of Ga-MFI at Ga K-edge. (g) K^3-weighted Fourier transform EXAFS spectrum of Ga-MFI. (h) Ga K-edge wavelet transform (WT)-EXAFS of $Ga_{2.61}$-MFI, Ga/S-1 and Ga_2O_3.

synthesized *via* ligand-modulated crystallization. The coupling conversion of cyclohexane (a model naphtha component) with CO_2 under moderate conditions realized efficient aromatics production. Time-resolved X-ray absorption spectroscopy reveals that the zeolite-confined Ga centers undergo reversible coordination switching between oxide and hydride states during the coupling conversion. Advanced microscopy further uncovers a critical spatial relationship between gallium sites and proximal Brønsted acid groups, where subnanometer proximity amplifies cooperative polarization of reactant molecules. Isotopic pulse experiments and operando mass spectrometry collectively disentangle the multifunctional role of CO_2. These insights collectively establish Ga-MFI as a dynamic single-site catalysis platform, bridging the mechanistic understanding with scalable strategies for CO_2-coupled hydrocarbon upgrading.

2. RESULTS AND DISCUSSION

2.1. Structure and Phase Analysis. The incorporation of gallium into MFI zeolites confers exceptional CO_2-coupled cyclohexane aromatization activity.[29,30] In this work, Ga-MFI catalysts with controlled Ga loadings (0.37−2.61 wt %) were synthesized *via* an ethylenediamine-assisted hydrothermal protocol (Figure S1). XRD analysis confirms Ga-MFI crystallization, with characteristic Bragg reflections showing systematic peak broadening at higher Ga contents (Figures 1a,b and S5 and Table S1). This distortion arises from the substitution of a smaller Si by a larger Ga in tetrahedral coordination.

Morphological characterization reveals uniform Ga-MFI nanoparticles (200−300 nm) with well-defined crystallinity, as evidenced by scanning electron microscope (SEM) imaging (Figure S2) and transmission electron microscopy (TEM) lattice fringe analysis (Figure S3). Atomic-resolution HAADF-STEM (Figure S4) combined with EDS mapping (Figure 1c,d) demonstrates the homogeneous distribution of Ga atoms within the MFI framework, with no detectable Ga clusters or secondary phases, which is a critical indicator of successful isomorphous substitution.

N_2 physisorption isotherms (Figure S6 and Table S2) confirm the microporous architecture of Ga-MFI, exhibiting characteristic Type I behavior with a BET surface area and pore volume. Acidic properties, probed through NH_3-TPD and pyridine-IR spectroscopy (Figure S7 and Table S3), reveal a

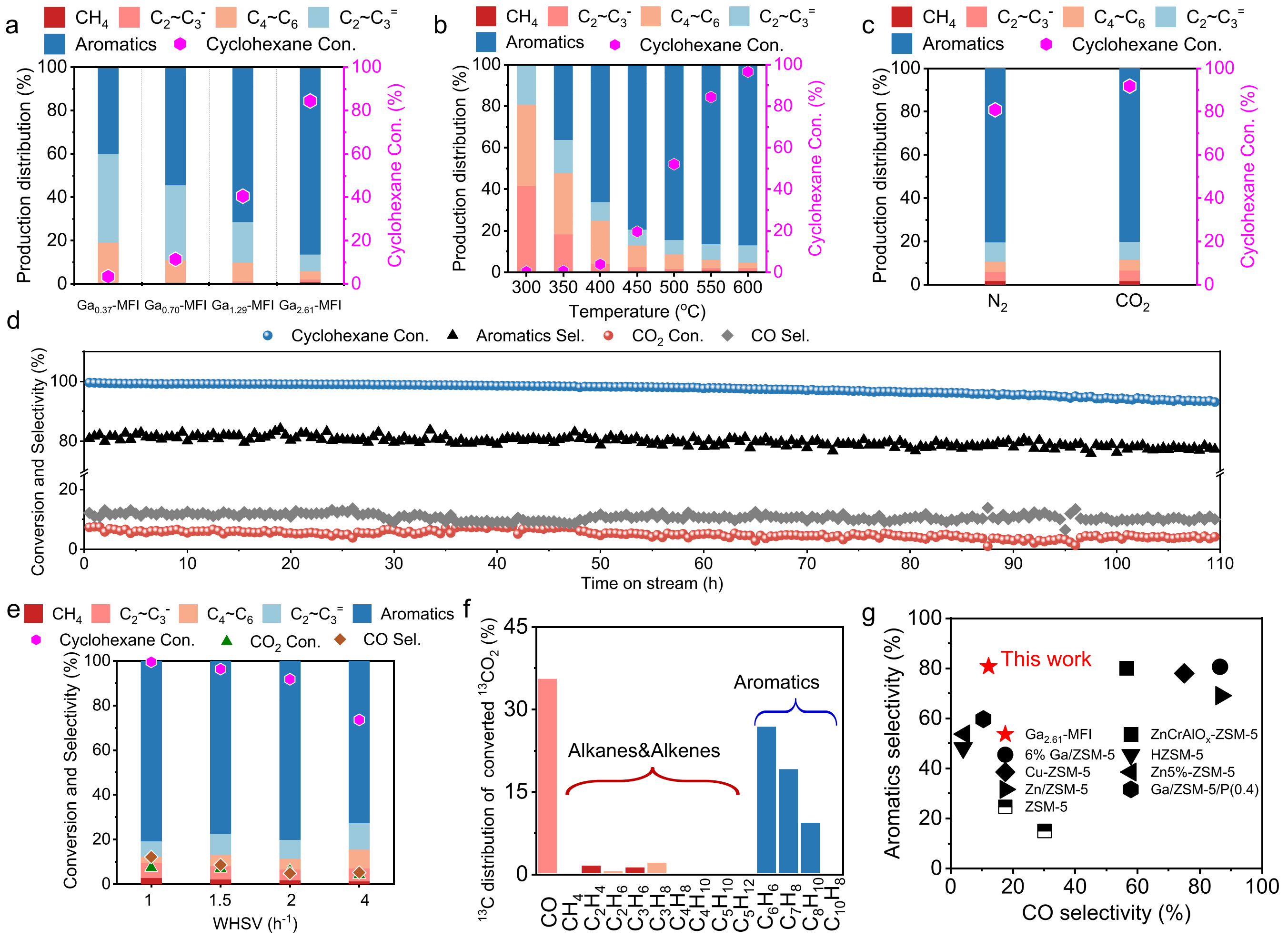

Figure 2. Catalytic performance of the Ga-MFI catalyst. (a) Effect of Ga contents on cyclohexane aromatization. (b) The impact of reaction temperature. (c) Comparison of cyclohexane aromatization and CO_2-coupled cyclohexane aromatization over $Ga_{2.61}$-MFI. (d) Durability test of the catalyst in the CO_2-coupled cyclohexane aromatization over $Ga_{2.61}$-MFI. (e) Effect of different space velocities in the CO_2-coupled cyclohexane aromatization over $Ga_{2.61}$-MFI. (f) $^{13}CO_2$ isotope tracer technology tracks the distribution of C in the products of CO_2 conversion. (g) The aromatics and CO selectivity in comparison to those reported.[9,14,15,17,28,36−38] Reaction conditions: (a) $T = 550$ °C, $P = 0.1$ MPa, WHSV = 2 h^{-1}, Ar: Cyclohexane = 10:1, $m_{cat.} = 0.25$ g. (b) $P = 0.1$ MPa, WHSV = 2 h^{-1}, Ar: cyclohexane = 10:1, $m_{cat.} = 0.25$ g, and $Ga_{2.61}$-MFI. (c) $T = 550$ °C, $P = 0.1$ MPa, WHSV = 2 h^{-1}, cyclohexane: CO_2: N_2 = 1:8:2, $m_{cat.} = 0.25$ g, $Ga_{2.61}$-MFI. (d) $T = 550$ °C, $P = 0.1$ MPa, cyclohexane: CO_2: N_2 = 1:8:2, $m_{cat.} = 0.25$ g, WHSV = 1 h^{-1}, $Ga_{2.61}$-MFI. (e) $T = 550$ °C, $P = 0.1$ MPa, cyclohexane: CO_2: N_2 = 1:8:2, $m_{cat.} = 0.25$ g, $Ga_{2.61}$-MFI. (f) $T = 550$ °C, $P = 0.1$ MPa, cyclohexane: CO_2: N_2 = 1:8:2, $m_{cat.} = 0.25$ g, WHSV = 2 h^{-1}, $Ga_{2.61}$-MFI.

Ga-dependent increase in total acid sites from 3.71 to 98.59 μmol/g and the varied Brønsted/Lewis acidity.

Fourier transform infrared (FTIR) spectroscopy (Figure 1e) was employed to probe surface functional groups and acid sites in Ga-MFI. Distinct vibrational bands at 3714 cm^{-1} (silanols) and 3593 cm^{-1} (Brønsted acid sites) confirm the coexistence of hydroxyl groups and protonic acid centers.[27,31] The broad FTIR band at ∼3500 cm^{-1} is attributed to perturbed silanol groups, likely due to framework distortion and partial silanol nest formation induced during Ga incorporation. The Brønsted acid signal intensity exhibits a Ga-loading-dependent enhancement, directly correlating with framework Ga species incorporation that generates protons for charge-compensating. This trend aligns with pyridine-IR spectroscopy and XRD data, demonstrating that the isomorphous Ga substitution tailors acidity.

X-ray absorption spectroscopy provides atomic-level insights into Ga coordination states. The Ga K-edge XANES spectra (Figure 1f) exhibit an absorption maximum at 10,374 eV, closely matching β-Ga_2O_3 references.[32,33] First-derivative edge energy analysis (Figure S8) confirms the oxidation state of framework Ga. Fourier transform EXAFS (Figure 1g) further differentiates the Ga-MFI environment from β-Ga_2O_3 controls, showing attenuated second-shell Ga−Si contributions that confirm framework incorporation over extra-framework clustering. Wavelet-transformed EXAFS (Figure 1h) resolves tetrahedral Ga−O coordination without detectable Ga−Ga paths.

The EXAFS spectra for both Ga-MFI and β-Ga_2O_3 exhibit prominent features in the first coordination shell. A distinct peak in β-Ga_2O_3 corresponds to Ga−Ga backscattering, while weaker features in the same region for Ga-MFI arise from Ga−Si interactions within the framework. Wavelet transforms of the k^3-weighted EXAFS spectra (Figures 1f−h and S9) reveal a dominant feature at 3.25 Å (r-space) and 7−10 $Å^{-1}$ (k-space), consistent with tetrahedrally coordinated Ga centers in Ga-MFI. Quantitative EXAFS fitting (Table S4 and Figures S10−S13) yields an average Ga−O bond length of 1.81 Å with tetrahedral coordination geometry. This contrasts sharply with β-Ga_2O_3 (mixed tetrahedral/octahedral sites)[34,35] and sup-

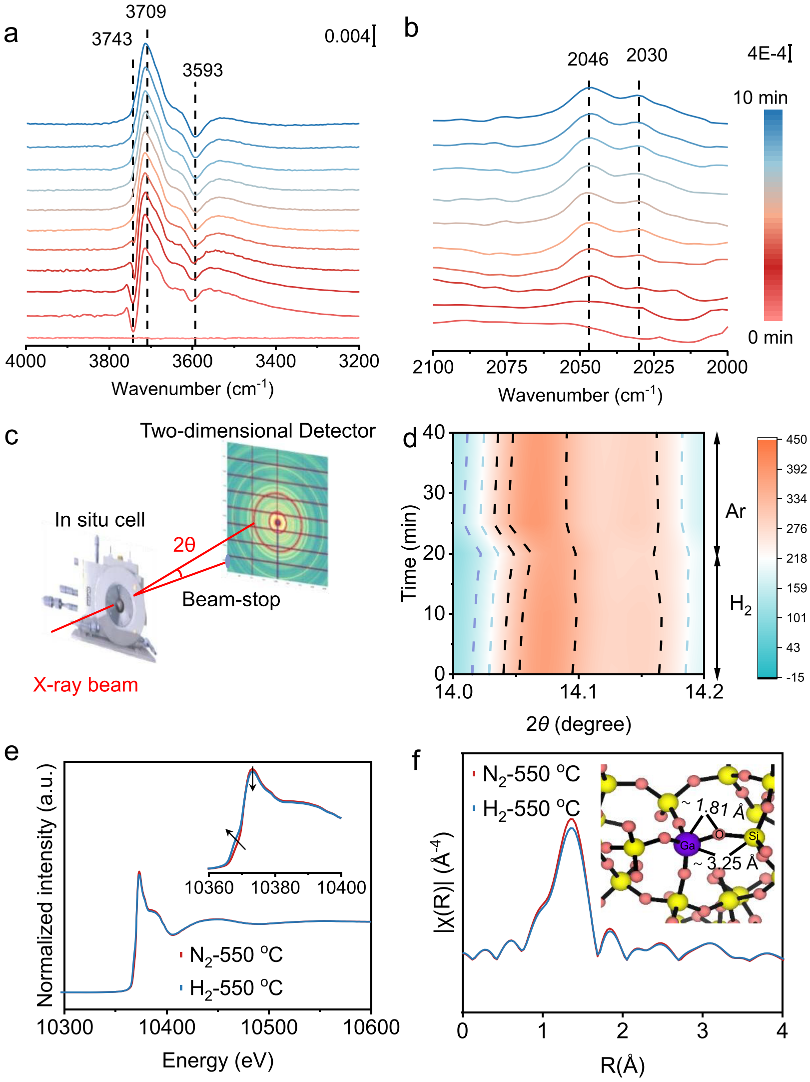

Figure 3. Dynamic evolution of catalysts. (a,b) *In situ* Fourier transform infrared (FTIR) spectra of $Ga_{2.61}$-MFI treated at 550 °C in H_2 atmosphere for 10 min. (c) Schematic diagram of *in situ* synchrotron radiation (SR) XRD. (d) *In situ* synchrotron radiation (SR) XRD patterns of $Ga_{2.61}$-MFI treated at 550 °C in H_2 atmosphere and Ar atmosphere. (e) XANES spectra of the Ga K-edge of $Ga_{2.61}$-MFI after H_2 reduction. (f) Fourier transform amplitude of Ga K-edge EXAFS spectra of $Ga_{2.61}$-MFI after H_2 reduction.

ported Ga/S-1 (disordered clusters), confirming tetrahedral coordination dominance in the MFI framework.

The integrated characterization protocol conclusively demonstrates that Ga-MFI possesses a well-defined crystalline architecture with atomically dispersed Ga centers in tetrahedral coordination, as evidenced by X-ray absorption spectroscopy (XAS) and HAADF-STEM analysis. Isomorphous substitution of Ga into the MFI framework induces dual functionality: (i) enhanced Brønsted acidity through Ga incorporation to generated bridge hydroxyl groups Ga−OH−Si, and (ii) modified electronic properties. These synergistic effects Ga-MFI as an archetypal single-site catalyst for demanding hydrocarbon transformations, particularly those requiring acid−redox bifunctionality.

2.2. Catalytic Performance. The CO_2-coupled cyclohexane aromatization reaction demonstrates CO_2 as a reactive participant. CO_2 shifts reaction equilibrium by consuming hydrogen through the reverse water−gas shift (RWGS) while simultaneously contributing to aromatic formation *via* oxygenate intermediates (Figure S14). Compared with the hydrogen reduction pretreatment, the treated catalyst did not maintain efficient conversion (Figure S15). As shown in Figure 2a and Table S5, catalytic activity exhibits pronounced Ga-loading dependence, peaking at 2.61 wt % Ga with 84.37% cyclohexane conversion and 86.34% aromatic selectivity. Temperature-dependent studies (Figure 2b) show cyclohexane conversion increasing from 52.02% (500 °C) to 96.59% (600 °C) while maintaining >80% aromatic selectivity.

The synergistic coupling of cyclohexane with CO_2 demonstrates exceptional efficacy for aromatic synthesis. As evidenced in Figure 2c, introducing CO_2 elevates cyclohexane conversion from 80.8% (N_2 atmosphere) to 91.76%. In addition, under certain conditions, increasing the feed ratio of CO_2 and cyclohexane can increase cyclohexane conversion (Figure S15). Kinetic analysis reveals an activation energy of 120.06 kJ/mol for cyclohexane dehydrogenation (Figure S15). Under 1 h^{-1} space velocity, almost complete cyclohexane conversion (99.57%) was achieved with 80.76% aromatic selectivity, achieving simultaneous high activity and product specificity rarely reported in thermal catalysis.

The Ga-MFI catalyst exhibits exceptional operational stability under optimized conditions, maintaining 94% cyclohexane conversion after 110 h of continuous operation—a mere 5.6% decline from the initial 99.6% conversion (Figure 2d). Postreaction thermogravimetric analysis quantifies coke deposition at 8 wt % (Figure S16). Pressure-dependent studies reveal a 22% reduction in aromatic selectivity when increasing from 0.1 to 2 MPa (Figure S15). Residence time optimization further demonstrates competing reaction networks: prolonging contact duration elevates alkane selectivity to 12.3% yet preserves 7.35% CO_2 conversion efficiency (Figure 2e).

To probe the hydrogenation functionality of Ga-MFI, CO_2 hydrogenation tests were conducted at varied temperatures and pressures (Figures S17 and S18). GC-MS analysis identifies methanol as a primary intermediate and subsequent alkane/aromatic formation *via* methanol-to-hydrocarbon pathways. This hydrogenation proficiency is further quantified through ^{13}C isotopic tracing: cofeeding $^{13}CO_2$ with unlabeled cyclohexane (Figure 2f) reveals 56.4% of aromatic carbon atoms originated from CO_2, directly verifying its incorporation into hydrocarbon chains. The calculation method of product isotopic distribution was similar to that reported by Dahl and Kolboe.[39] Compared with the reported ones, it has obvious advantages in the selectivity of aromatics and CO (Figure 2g).

The catalyst is underscored through naphtha feedstock trials (Figure S19). For cycloalkane-rich feeds (72% methyl cyclopentane, 18% cyclohexane), the total aromatic and olefin selectivity reaches 88.4% at WHSV = 1 h^{-1}, outperforming linear alkane-dominated feeds (65% *n*-hexane), where selectivity is 81%. These results collectively validate the versatility of Ga-MFI in processing complex hydrocarbon mixtures while maintaining a CO_2 utilization efficiency.

2.3. Identification of Active Sites. The transformation of Ga to hydridic species under H_2 treatment was systematically characterized by using *in situ* Fourier transform infrared (FTIR) spectroscopy. Prior to reduction, dehydrated Ga-MFI exhibits distinct vibrational signatures at 3709 cm^{-1} (Si−OH silanols) and 3593 cm^{-1} (bridged Brønsted acid sites, BAS), as shown in Figure 1e. Exposure to H_2 at 550 °C (1 atm) triggers the emergence of new peaks at 2046 cm^{-1} and 2030 cm^{-1}, which are assigned to $[GaH]^{2+}$ and $[GaH_2]^+$ species,[40,41] respectively. The simultaneous reduction of BAS-related vibrations at 3593 cm^{-1} and the enhanced intensity of Si−OH stretching modes at 3709 cm^{-1} suggest the cleavage of Ga−O bonds and subsequent formation of GaH_x species (Figure 3a,b). These Ga hydrides remain relatively long for a period of time under inert Ar atmospheres but undergo rapid degradation upon CO_2 introduction, concomitant with CO production, directly linking GaH_x species to CO_2 activation. Hydride regeneration rates exhibit temperature dependence, with higher reduction temperatures accelerating GaH_x formation. Sequential reduction cycles reveal GaH_x signal intensity (Figures S20−S25), indicative of Ga redistribution rather than permanent site loss. To further validate the role of Ga sites in hydrogen activation, complementary H−D exchange experiments (Figure S26) demonstrate their capacity for hydrogen adsorption and dissociation, consistent with the hydride-mediated catalytic cycle. Bulk H_2-TPR measurements (Figure S27) show no evidence of conventional redox behavior; however, *in situ* spectroscopy reveals a local transformation from Ga−O to Ga−H. Collectively, these results establish that the catalytic prowess of Ga-MFI stems from synergistic interactions between persistent acid sites and transient Ga hydrides, rather than from isolated redox-active centers. Figures 3c,3d and S28 and S29 illustrate the evolution of active sites in Ga-MFI zeolite through *in situ* synchrotron radiation X-ray diffraction (SR-XRD) analysis under H_2 reduction conditions. The sample was exposed to a 10 vol % H_2/Ar mixed gas to monitor dynamic changes in its crystal structure. The results showed that while the diffraction peak intensity of the MFI phase in Ga-MFI remained stable under the high-temperature reducing environment, indicating high crystal structure stability, the diffraction peak position shifted to a higher angle (Figure 3d). This shift reflects a slight decrease in the unit cell parameters, which may be linked to the reduction of Ga species and the release of framework stress during the H_2 reduction process (Figure 3d). This suggests that Ga species might have partially migrated, thereby altering the local environment of the active sites. When the H_2 reduction was halted and replaced with a pure Ar purge, the diffraction peak position gradually returned to its initial state, indicating that the change in the unit cell parameters was reversible. This phenomenon highlights that the structural changes induced during the reduction process are dynamic,[42,43] likely due to the transformation of Ga species within the framework and the self-recovery properties of the local structure. This dynamic process emphasizes the structural and chemical transformations of active sites under different reactive atmospheres in Ga-MFI, offering insights into further optimizing its catalytic performance. Combined with subsequent XANES and EXAFS analyses, the oxidation state transition of Ga and its relationship with structural changes in the active sites can be further explored, providing a more comprehensive understanding of the active site regulation mechanism in Ga-MFI under reducing conditions. *In situ* X-ray absorption near-edge structure (XANES) analysis of Ga-MFI after H_2 treatment (Figure 3e) reveals detailed redox behavior: while the Ga K-edge absorption maximum remains stable at 10368.9 eV, indicating framework-incorporated Ga species, the edge energy shift of 1.5 eV and the weakened white line intensity signal indicated the formation of GaH_x species formation (Figures S30 and S31). This phenomenon aligns with the established ligand substitution trends in the coordination sphere of Ga-MFI, where replacing one oxygen ligand with a σ-donating hydride reduces edge energy.[32] A decrease in coordination number from 3.21 Å (T = 550 °C, Ar) to 2.98 Å (T = 550 °C, H_2) induces an additional 1.5 eV red shift, collectively explaining the observed spectral evolution.

In situ EXAFS analysis (Figure 3f) further reveals local structural changes in Ga species within Ga-MFI during H_2 treatment. The Fourier-transformed Ga K-edge EXAFS spectrum shows a marked decrease in the intensity of the Ga−O bond after H_2 treatment, indicating a reduction in the coordination number of the Ga site. The fitting results also reveal that the coordination number of Ga−O decreases from 3.21 Å (T = 550 °C, Ar) to 2.98 Å (T = 550 °C, H_2), suggesting the partial replacement of oxygen ligands by hydride (H^-). Additionally, a new characteristic peak is observed in the Fourier transform spectrum, likely corresponding to the Ga−H bond, further confirming the formation of the $[GaH_2]^+$ species. The EXAFS data indicate that the Ga species undergoes a structural reorganization in the H_2 environment, consistent with the observed decrease in the absorption peak position in the XANES spectra. Notably, despite changes in the coordination environment, Ga remains within the molecular sieve framework, indicating that the H_2 treatment primarily triggers coordination adjustments rather than migration or

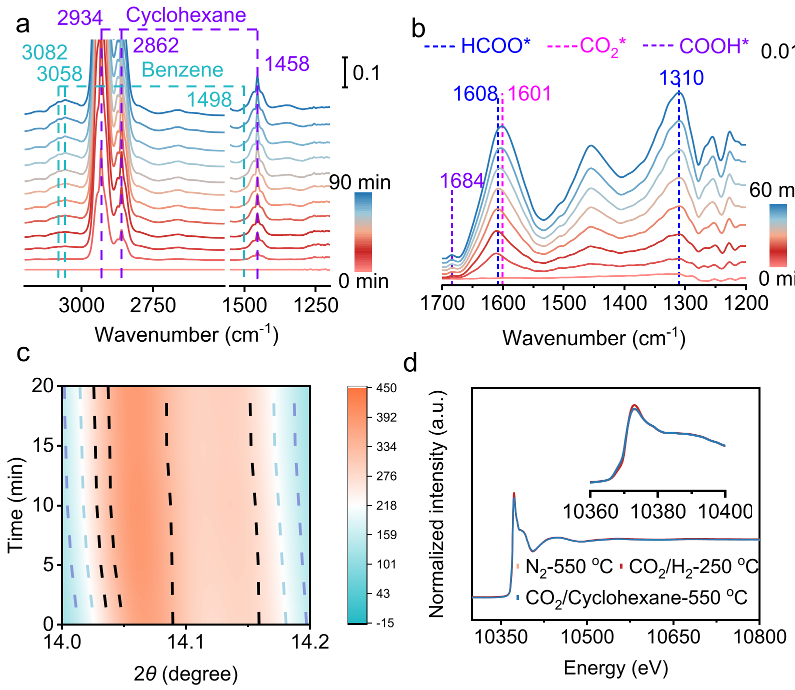

Figure 4. Mechanism of the Ga-MFI catalyst under working conditions. (a) *In situ* Fourier transform infrared (FTIR) spectrum of Ga-MFI in a cyclohexane atmosphere at 550 °C. (b) *In situ* Fourier transform infrared (FTIR) spectroscopy of Ga-MFI in a CO_2/H_2 atmosphere at 250 °C. (c) *In situ* synchrotron radiation (SR) XRD patterns in a CO_2/cyclohexane atmosphere at 550 °C. (d) *In situ* XANES spectra in a CO_2/H_2 atmosphere at 250 °C and a CO_2/cyclohexane atmosphere at 550 °C.

complete reduction of Ga species. Table S4 presents the detailed fitting analysis of the first and second coordination shells from which bond lengths for Ga−O and Ga−Si can be inferred, supporting the formation of GaH_x species and suggesting that they may serve as catalytic active centers.

In situ EXAFS analysis (Figure 3f) elucidates the dynamic coordination evolution of the Ga species in Ga-MFI during H_2 treatment. Fourier transform analysis of Ga K-edge EXAFS spectra quantifies progressive ligand substitution: the Ga−O coordination number decreases from 3.21 Å (T = 550 °C, Ar) to 2.98 Å (T = 550 °C, H_2) (Table S4). Quantitative bond length analysis (Table S4) resolves emerging Ga−O bonds at 1.76 Å and preserved Ga−Si interactions at 2.94 Å. These reversible coordination adjustments, distinct from permanent structural degradation, establishing GaH_x centers as dynamic active sites for H-mediated catalysis.

2.4. Reaction Mechanism. The dynamic evolution of the active centers of Ga-MFI under operando conditions was decoupled through integrated *in situ* characterizations: synchronized FTIR analyses, synchrotron XRD (SR-XRD), and XAFS-mass spectrometry (XAFS-MS). *In situ* FTIR spectroscopy reveals mechanistic insights into the cyclohexane−CO_2 coupling process. Under Ar atmosphere (Figure 4a), adsorbed cyclohexane exhibits characteristic C−H vibrations at 2934 cm^{-1}, 2862 cm^{-1}, and 1458 cm^{-1}, with aromatic C−H vibrations at 3082 cm^{-1}, 3058 cm^{-1}, and 1498 cm^{-1},[44,45] consistent with NIST reference spectra. Introducing CO_2 generates gas-phase signals at 3740 cm^{-1}, 3700 cm^{-1}, 3630 cm^{-1}, and 3595 cm^{-1}, alongside a distinct 2178 cm^{-1} band indicative of CO formation, while oxygenates like lactones/cycloalkenones remain undetected (Figure S32). Isotopic switching with $^{13}CO_2$ induces 85 cm^{-1} and 40 cm^{-1} red shifts for CO_2 from 3595 to 3510 cm^{-1} and for CO from 2178 to 2119 cm^{-1}, respectively (Figure S33). In CO_2 and hydrogen atmosphere (Figures 4b and S34 and S35) further identify adsorbed intermediates: 1608 cm^{-1} (ν_{as}OCO, HCOO*), 1684 cm^{-1} (νC═O, COOH*), and 2964 cm^{-1} (νC−H, CH_3O*) with the formation of methanol.[46,47] The captured adsorbed species further determined the feasibility of the methanol route, corresponding to the GC-MS results. These results collectively validate the bifunctional capacity of Ga-MFI to activate C−H bonds and reduce CO_2.

In situ SR-XRD tracks reversible lattice dynamics: H_2-reduced Ga-MFI maintains GaH_x-associated lattice contraction (Figure S36), while CO_2 exposure triggers transient expansion as GaH_x regenerates (Figure 4c). This oscillatory structural response, with contraction/expansion cycles within 2% lattice strain, confirms the dynamic equilibrium between GaH_x formation (H_2 activation) and its consumption through hydrogenation at 250 °C (Figure 4d), coinciding with methanol detection by mass spectrometry, directly demonstrating GaH_x-mediated Ga reduction (Figures S37−S40). Subsequent cyclohexane−CO_2 coupling induces partial GaH_x oxidation, generating CO *via* $GaH_x + CO_2 \rightarrow$ Ga−O−CO + H_2O pathways.

The reaction pathway for cyclohexane−CO_2 coupling over the Ga-MFI zeolite (Figure 5) integrates evidence from *in situ* FTIR and isotopic labeling. Cyclohexane is activated at the Brønsted acid sites and converted to aromatics. With the introduction of CO_2, the reverse water−gas shift reaction facilitates hydrogen elimination, significantly enhancing cyclohexane conversion to 91.76%. The characteristic CO vibration at 2178 cm^{-1} and an 85 cm^{-1} red shift upon $^{13}CO_2$ introduction confirm CO_2 conversion to CO. At lower temperatures (<550 °C), CO_2 hydrogenation generates C_2−C_4 olefins, which further participate in aromatic formation *via* H-transfer. At elevated temperatures, GaH_x species mediate direct CO_2 carboxylation, suppressing oxygenate byproducts

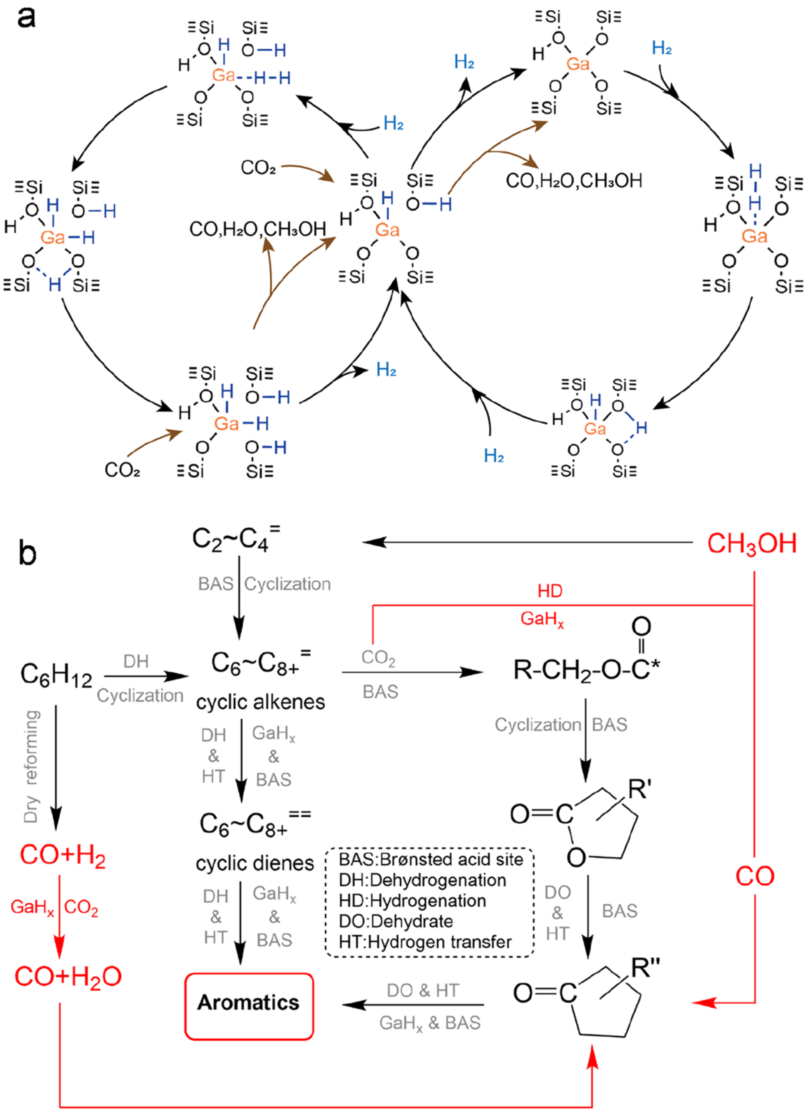

Figure 5. Mechanism illustration. (a) Dynamic transformation of Ga-MFI active centers and the pathway of CO_2 participation (from *in situ* FTIR, XANES, EXAFS, and GC-MS). (b) Schematic depiction of the reaction network for the cyclohexane−CO_2 coupling process.

(no lactone/cycloalkenone signals in the 1600−1800 cm^{-1} range). This bifunctional mechanism synergistically enhances aromatic production while maintaining alkane selectivity below 12.3%, highlighting Ga-MFI's unique capability in C−H activation and CO_2 utilization.

3. CONCLUSIONS

This work demonstrates the successful incorporation of isolated Ga species within the MFI zeolite framework, characterized by a distorted tetrahedral configuration $\{(\equiv SiO)_3Ga(HO-Si\equiv)\}$ as confirmed through SEM, TEM, XAS, and FTIR spectroscopy. Under optimized conditions, $Ga_{2.61}$−MFI catalyzes efficient coupling conversion of CO_2 and cyclohexane, predominantly yielding aromatics (80.76% selectivity) while minimizing alkane byproducts (<12.3%). Isotopic tracing and *in situ* analyses reveal that 56.4% of aromatic carbon originates from CO_2. The catalyst exhibits exceptional stability, retaining 94% initial activity after 110 h with negligible coking (8 wt %), attributed to the dynamic structure of framework-anchored Ga species and the role of CO_2 in removing carbon deposits. *In situ* XAS and FTIR studies elucidate dynamic Ga speciation involving reversible coordination switching between oxidized (Ga−O) and reduced (Ga−H) states, which facilitates sequential C−H activation and C═O bond cleavage. This dual-functional mechanism, synergizing Brønsted acid sites and redox-active Ga centers, enables efficient adsorption, bond dissociation, and dehydrogenation steps critical for sustaining catalytic cycles. These findings establish a scalable strategy for designing stable, coke-resistant zeolite catalysts, advancing CO_2 utilization, and alkane valorization.

■ ASSOCIATED CONTENT

Supporting Information

The Supporting Information is available free of charge at https://pubs.acs.org/doi/10.1021/jacs.5c09737.

Experimental section; and additional data for catalyst characterization and reactions (PDF)

AUTHOR INFORMATION

Corresponding Authors

Jingfeng Han − *National Engineering Research Center of Lower-Carbon Catalysis Technology, Dalian National Laboratory for Clean Energy, Dalian Institute of Chemical Physics, Chinese Academy of Sciences, Dalian 116023, China;* orcid.org/0000-0001-7775-4183; Email: jfhan@dicp.ac.cn

Zhongmin Liu − *National Engineering Research Center of Lower-Carbon Catalysis Technology, Dalian National Laboratory for Clean Energy, Dalian Institute of Chemical Physics, Chinese Academy of Sciences, Dalian 116023, China;* orcid.org/0000-0002-7999-2940; Email: liuzm@dicp.ac.cn

Authors

Haohao Feng − *National Engineering Research Center of Lower-Carbon Catalysis Technology, Dalian National Laboratory for Clean Energy, Dalian Institute of Chemical Physics, Chinese Academy of Sciences, Dalian 116023, China; University of Chinese Academy of Sciences, Chinese Academy of Sciences, Beijing 100049, China*

Zhong-Pan Hu − *National Engineering Research Center of Lower-Carbon Catalysis Technology, Dalian National Laboratory for Clean Energy, Dalian Institute of Chemical Physics, Chinese Academy of Sciences, Dalian 116023, China*

Enze Chen − *National Engineering Research Center of Lower-Carbon Catalysis Technology, Dalian National Laboratory for Clean Energy, Dalian Institute of Chemical Physics, Chinese Academy of Sciences, Dalian 116023, China; University of Chinese Academy of Sciences, Chinese Academy of Sciences, Beijing 100049, China*

Yimo Wu − *National Engineering Research Center of Lower-Carbon Catalysis Technology, Dalian National Laboratory for Clean Energy, Dalian Institute of Chemical Physics, Chinese Academy of Sciences, Dalian 116023, China;* orcid.org/0000-0002-7319-8260

Min Li − *University of Bologna, Dept Ind Chem Toso Montanari, I-40136 Bologna, Italy*

Yingxu Wei − *National Engineering Research Center of Lower-Carbon Catalysis Technology, Dalian National Laboratory for Clean Energy, Dalian Institute of Chemical Physics, Chinese Academy of Sciences, Dalian 116023, China;* orcid.org/0000-0002-0412-1980

Complete contact information is available at:
https://pubs.acs.org/10.1021/jacs.5c09737

Author Contributions

This paper contains extensive contributions from all authors. All authors have given approval to the final version of the manuscript.

Notes

The authors declare no competing financial interest.

ACKNOWLEDGMENTS

This work was supported by the National Key Research and Development Program of China (No. 2022YFE0116000), the National Natural Science Foundation of China (Nos. 22202193, 22172166, and 22288101), the Excellent Research Assistant Funding Project of CAS, the Youth Innovation Promotion Association CAS (2021182), the Innovation Research Foundation of Dalian Institute of Chemical Physics, Chinese Academy of Sciences (DICP I202217). We thank the BL14W and BL17UM beamline at the Shanghai Synchrotron Radiation Facility (https://cstr.cn/31124.02.SSRF. BL14W and https://cstr.cn/31124.02.SSRF. BL17UM) for the XAFS and SR-XRD experiments supports.

REFERENCES

(1) Ciapetta, F. G.; Wallace, D. N. Catalytic Naphtha Reforming. *Catal. Rev.* **1972**, *5* (1), 67−158.

(2) Akhtar, M. N.; Aitani, A. M.; Ummer, A. C.; Alasiri, H. S. Review on the Catalytic Conversion of Naphtha to Aromatics: Advances and Outlook. *Energy Fuels* **2023**, *37* (4), 2586−2607.

(3) Aitani, A.; Akhtar, M. N.; Al-Khattaf, S.; Jin, Y.; Koseoglu, O.; Klein, M. T. Correction to Catalytic Upgrading of Light Naphtha to Gasoline Blending Components: A Mini Review. *Energy Fuels* **2020**, *34* (2), 2617.

(4) Sterba, M. J.; Haensel, V. Catalytic Reforming. *Ind. Eng. Chem. Prod. Res. Dev.* **1976**, *15* (1), 2−17.

(5) Wang, D.; Wei, X.; Shou, S.; Gong, J. Dealkylation in Fluid Catalytic Cracking Condition for Efficient Conversion of Heavy Aromatics to Benzene−Toluene−Xylene. *ACS Omega* **2023**, *8* (12), 10789−10795.

(6) Tomás, R. A. F.; Bordado, J. C.; Gomes, J. F. p-Xylene oxidation to terephthalic acid: a literature review oriented toward process optimization and development. *Chem. Rev.* **2013**, *113* (10), 7421−7469.

(7) Hagemeyer, A.; Borade, R.; Desrosiers, P.; Guan, S.; Lowe, D. M.; Poojary, D. M.; Turner, H.; Weinberg, H.; Zhou, X.; Armbrust, R.; Fengler, G.; Notheis, U. Application of combinatorial catalysis for the direct amination of benzene to aniline. *Appl. Catal., A* **2002**, *227* (1), 43−61.

(8) Guo, X.; Fang, G.; Li, G.; Ma, H.; Fan, H.; Yu, L.; Ma, C.; Wu, X.; Deng, D.; Wei, M.; Tan, D.; Si, R.; Zhang, S.; Li, J.; Sun, L.; Tang, Z.; Pan, X.; Bao, X. Direct, Nonoxidative Conversion of Methane to Ethylene, Aromatics, and Hydrogen. *Science* **2014**, *344* (6184), 616−619.

(9) Gomez, E.; Nie, X.; Lee, J. H.; Xie, Z.; Chen, J. G. Tandem Reactions of CO_2 Reduction and Ethane Aromatization. *J. Am. Chem. Soc.* **2019**, *141* (44), 17771−17782.

(10) Jin, X.; Ding, J.; Xia, Q.; Zhang, G.; Yang, C.; Shen, J.; Subramaniam, B.; Chaudhari, R. V. Catalytic conversion of CO_2 and shale gas-derived substrates into saturated carbonates and derivatives: Catalyst design, performances and reaction mechanism. *J. CO_2 Util.* **2019**, *34*, 115−148.

(11) Snoeckx, R.; Bogaerts, A. Plasma technology − a novel solution for CO_2 conversion? *Chem. Soc. Rev.* **2017**, *46* (19), 5805−5863.

(12) Zhai, P.; Xie, Z.; Huang, E.; Aireddy, D. R.; Yu, H.; Cullen, D. A.; Liu, P.; Chen, J. G.; Ding, K. CO_2-mediated oxidative dehydrogenation of propane enabled by Pt-based bimetallic catalysts. *Chem.* **2023**, *9* (11), 3268−3285.

(13) Xie, Z.; Wang, X.; Chen, X.; Liu, P.; Chen, J. G. General Descriptors for CO_2-Assisted Selective C−H/C−C Bond Scission in Ethane. *J. Am. Chem. Soc.* **2022**, *144* (9), 4186−4195.

(14) Ren, X.; Hu, Z.-P.; Han, J.; Wei, Y.; Liu, Z. Enhancing the aromatic selectivity of cyclohexane aromatization by CO_2 coupling. *Front. Chem. Sci. Eng.* **2023**, *17*, 1801−1808.

(15) Sun, X.; Liu, R.; Fan, G.; Liu, Y.; Ye, F.; Yu, Z.; Liu, Z. Understanding the correlation between zinc speciation and coupling conversion of CO_2 and n-butane on zinc/ZSM-5 catalysts. *Chin. J. Catal.* **2024**, *61*, 154−163.

(16) Wei, C.; Zhang, W.; Yang, K.; Bai, X.; Xu, S.; Li, J.; Liu, Z. An efficient way to use CO_2 as chemical feedstock by coupling with alkanes. *Chin. J. Catal.* **2023**, *47*, 138−149.

(17) Yang, K.; Li, J.; Wei, C.; Zhao, Z.; Liu, Z. Coupling Conversion of CO_2 and n-Butane Over Modified ZSM-5: Incorporation of the Carbon from CO_2 into Hydrocarbon Products. *ACS Catal.* **2023**, *13* (15), 10405−10417.

(18) Xie, Z.; Yan, B.; Lee, J. H.; Wu, Q.; Li, X.; Zhao, B.; Su, D.; Zhang, L.; Chen, J. G. Effects of oxide supports on the CO_2 reforming of ethane over Pt-Ni bimetallic catalysts. *Appl. Catal., B* **2019**, *245*, 376−388.

(19) Xing, F.; Ma, J.; Shimizu, K.-i.; Furukawa, S. High-entropy intermetallics on ceria as efficient catalysts for the oxidative dehydrogenation of propane using CO_2. *Nat. Commun.* **2022**, *13* (1), No. 5065.

(20) Xing, F.; Nakaya, Y.; Yasumura, S.; Shimizu, K.-i.; Furukawa, S. Ternary platinum−cobalt−indium nanoalloy on ceria as a highly efficient catalyst for the oxidative dehydrogenation of propane using CO_2. *Nat. Catal.* **2022**, *5* (1), 55−65.

(21) Zhao, L.; Qin, X.; Zhang, X.; Cai, X.; Huang, F.; Jia, Z.; Diao, J.; Xiao, D.; Jiang, Z.; Lu, R.; Wang, N.; Liu, H.; Ma, D. A Magnetically Separable Pd Single-Atom Catalyst for Efficient Selective Hydrogenation of Phenylacetylene. *Adv. Mater.* **2022**, *34* (20), No. 2110455.

(22) Asaftei, I. V.; Lungu, N. C.; Birsa, L.; Sarbu, L.; Ignat, M. Conversion of light hydrocarbons from petroleum refining processes over Zn-HZSM-5 (nitrate) and Zn-HZSM-5 (acetate) A comparative study. *Rev. Chim.* **2016**, *67*, 1523−1528.

(23) Yan, T.; Zhang, M.; Liu, R.; Dai, W.; Guan, N.; Li, L. Acetone−Butanol−Ethanol Catalytic Upgrading into Aromatics over Ga-Modified HZSM-5 Zeolites. *ACS Catal.* **2023**, *13* (10), 7087−7102.

(24) Sun, G.; Zhao, Z.-J.; Li, L.; Pei, C.; Chang, X.; Chen, S.; Zhang, T.; Tian, K.; Sun, S.; Zheng, L.; Gong, J. Metastable gallium hydride mediates propane dehydrogenation on H_2 co-feeding. *Nat. Chem.* **2024**, *16* (4), 575−583.

(25) Kazansky, V. B.; Subbotina, I. R.; van Santen, R. A.; Hensen, E. J. M. DRIFTS study of the nature and chemical reactivity of gallium ions in Ga/ZSM-5: II. Oxidation of reduced Ga species in ZSM-5 by nitrous oxide or water. *J. Catal.* **2005**, *233* (2), 351−358.

(26) Niu, X.; Nie, X.; Yang, C.; Chen, J. G. CO_2-Assisted propane aromatization over phosphorus-modified Ga/ZSM-5 catalysts. *Catal. Sci. Technol.* **2020**, *10* (6), 1881−1888.

(27) Yuan, Y.; Brady, C.; Annamalai, L.; Lobo, R. F.; Xu, B.; et al. Ga speciation in Ga/H-ZSM-5 by in-situ transmission FTIR spectroscopy. *J. Catal.* **2021**, *393*, 60−69.

(28) Song, Y.; Hu, Z.-P.; Feng, H.; Chen, E.; Lv, L.; Wu, Y.; Liu, Z.; Jiang, Y.; Su, X.; Xu, F.; Zhu, M.; Han, J.; Wei, Y.; Mintova, S.; Liu, Z. The dynamic catalysis of Ga/ZSM-5 catalysts for propane-CO_2 coupling conversion to aromatics and syngas. *J. Energy Chem.* **2024**, *97*, 513−519.

(29) Mansoor, E.; Head-Gordon, M.; Bell, A. T. Computational Modeling of the Nature and Role of Ga Species for Light Alkane Dehydrogenation Catalyzed by Ga/H-MFI. *ACS Catal.* **2018**, *8* (7), 6146−6162.

(30) Kim, W.-g.; So, J.; Choi, S.-W.; Liu, Y.; Dixit, R. S.; Sievers, C.; Sholl, D. S.; Nair, S.; Jones, C. W. Hierarchical Ga-MFI Catalysts for Propane Dehydrogenation. *Chem. Mater.* **2017**, *29* (17), 7213−7222.

(31) Hu, Z. P.; Qin, G.; Han, J.; Zhang, W.; Wang, N.; Zheng, Y.; Jiang, Q.; Ji, T.; Yuan, Z. Y.; Xiao, J.; Wei, Y.; Liu, Z. Atomic Insight into the Local Structure and Microenvironment of Isolated Co-Motifs in MFI Zeolite Frameworks for Propane Dehydrogenation. *J. Am. Chem. Soc.* **2022**, *144* (27), 12127−12137.

(32) Phadke, N. M.; Van der Mynsbrugge, J.; Mansoor, E.; Getsoian, A. B.; Head-Gordon, M.; Bell, A. T. Characterization of Isolated Ga^{3+} Cations in Ga/H-MFI Prepared by Vapor-Phase Exchange of H-MFI Zeolite with $GaCl_3$. *ACS Catal.* **2018**, *8* (7), 6106−6126.

(33) Faro, A. C.; Rodrigues, V. d. O.; Eon, J.-G. In Situ X-ray Absorption Study of the Genesis and Nature of the Reduced Gallium Species in Ga/HZSM5 Catalysts. *J. Phys. Chem. A* **2011**, *115* (11), 4749−4756.

(34) Chen, H.; Gao, P.; Liu, Z.; Liang, L.; Han, Q.; Wang, Z.; Chen, K.; Zhao, Z.; Guo, M.; Liu, X.; Han, X.; Bao, X.; Hou, G. Direct Detection of Reactive Gallium-Hydride Species on the Ga_2O_3 Surface via Solid-State NMR Spectroscopy. *J. Am. Chem. Soc.* **2022**, *144* (38), 17365−17375.

(35) Ahman, J.; Svensson, G.; Albertsson, J. Reinvestigation of β-Gallium Oxide. *Acta Crystallogr., Sect. C:Cryst. Struct. Commun.* **1996**, *52* (6), 1336−1338.

(36) Ihm, S.-K.; Park, Y.-K.; Lee, S.-W. Effects of CO_2 addition on the aromatization of propane over metal-loaded ZSM-5 catalysts. *Appl. Organomet. Chem.* **2000**, *14* (12), 778−782.

(37) Fan, G.; Liu, R.; Zhao, Y.; Chen, E.; Yan, S.; Han, J.; Liu, J.; Yu, Z.; Liu, Z. CO_2-enhanced alkane aromatization over Cu-ZSM-5 zeolite: Insights into active sites and catalytic performance. *J. Energy Chem.* **2025**, *106*, 600−607.

(38) Shao, Y.; Ding, Y.; Jiao, F.; Miao, D.; Guo, S.; Wang, J.; Pan, X. CO_2 facilitated aromatization of butenes to benzene, toluene and xylene. *Catal. Today* **2025**, *454*, No. 115285.

(39) Dahl, I. M.; Kolboe, S. On the reaction-mechanism for propene formation in the mto reaction over sapo-34. *Catal. Lett.* **1993**, *20* (3−4), 329−336.

(40) Liu, Y.; Zhang, G.; Wang, J.; Zhu, J.; Zhang, X.; Miller, J. T.; Song, C.; Guo, X. Promoting propane dehydrogenation with CO_2 over Ga_2O_3/SiO_2 by eliminating Ga-hydrides. *Chin. J. Catal.* **2021**, *42* (12), 2225−2233.

(41) Zhou, Y.; Thirumalai, H.; Smith, S. K.; Whitmire, K. H.; Liu, J.; Frenkel, A. I.; Grabow, L. C.; Rimer, J. D. Ethylene Dehydroaromatization over Ga-ZSM-5 Catalysts: Nature and Role of Gallium Speciation. *Angew. Chem., Int. Ed.* **2020**, *59* (44), 19592−19601.

(42) Wang, W.; Chen, S.; Pei, C.; Luo, R.; Sun, J.; Song, H.; Sun, G.; Wang, X.; Zhao, Z.-J.; Gong, J. Tandem propane dehydrogenation and surface oxidation catalysts for selective propylene synthesis. *Science* **2023**, *381* (6660), 886−890.

(43) Yue, Y.; Wang, S.; Zhou, Q.; Wang, B.; Jin, C.; Chang, R.; Wan, L.; Pan, Z.; Zhu, Y.; Zhao, J.; Li, X. Tailoring Asymmetric Cu-O-P Coupling Site by Carbothermal Shock Method for Efficient Vinyl Chloride Synthesis over Carbon Supported Cu Catalysts. *ACS Catal.* **2023**, *13* (14), 9777−9791.

(44) Shang, X.; Liu, G.; Su, X.; Huang, Y.; Zhang, T. Preferential Synthesis of Toluene and Xylene from CO_2 Hydrogenation in the Presence of Benzene through an Enhanced Coupling Reaction. *ACS Catal.* **2022**, *12* (21), 13741−13754.

(45) Wang, H.; Wang, S.; Liu, S.; Dai, Y.; Jia, Z.; Li, X.; Liu, S.; Dang, F.; Smith, K. J.; Nie, X.; Hou, S.; Guo, X. Redox-induced controllable engineering of MnO_2-$MnxCo_{3\text{-}x}O_4$ interface to boost catalytic oxidation of ethane. *Nat. Commun.* **2024**, *15* (1), No. 4118.

(46) Shang, X.; Han, Q.; Zhang, W.; Wei, Y.; Liu, G.; Hou, G.; Su, X.; Huang, Y.; Zhang, T. Methoxy-bridged tandem CO_2 hydrogenation and ethylbenzene alkylation for selective synthesis of para-ethyl-toluene. *Appl. Catal., B* **2024**, *348*, No. 123833.

(47) Zuo, J.; Liu, C.; Han, X.; Wen, D.; Liu, X.; Ye, L.; Zhuang, W.; Yuan, Y. Steering CO_2 hydrogenation coupled with benzene alkylation toward ethylbenzene and propylbenzene using a dual-bed catalyst system. *Chem. Catal.* **2022**, *2* (5), 1223−1240.